1   Ammonia excretion in *Caenorhabditis elegans*: Physiological and

2   molecular characterization of the *rhr-2* knock-out mutant.

3

4

5   [$]Aida Adlimoghaddam, [#]Michael J. O'Donnell, [$]Jay Kormish, [$]Sheena Banh, [$]Jason R. Treberg,

6   [$]David Merz and [$][*]Dirk Weihrauch

7

8   [$]University of Manitoba, MB, Canada, [#]McMaster University, ON, Canada

9   [*]Corresponding author, email: Dirk.weihrauch@ad.umanitoba.ca

10

11

12

13

14

15

16

17

18

19 **Abstract**

20 Previous studies have shown the free living soil nematode *Caenorhabditis elegans* (N2 strain) to

21 be ammonotelic. Ammonia excretion was suggested to take place partially *via* the hypodermis,

22 involving the Na^+/K^+-ATPase (NKA), V-ATPase (VAT), carbonic anhydrase, NHX-3 and a

23 functional microtubule network and at least one Rh-like ammonia transporter RHR-1. In the

24 current study we show that a second Rh-protein, RHR-2, is highly expressed in the hypodermis,

25 here also in the apical membrane of that tissue. To further characterize the role of RHR-2 in

26 ammonia excretion, a knock-out mutant *rhr-2*(*ok403*), further referred to as Δ*rhr-2,* was

27 employed. Compared to wild-type worms (N2), this mutant showed a lower rate of ammonia

28 excretion and a lower hypodermal H^+ excretion rate. At the same time *rhr-1*, *nka*, *vat*, and *nhx-3*

29 showed higher mRNA expression levels when compared to N2. Also, in contrast to N2 worms,

30 Δ*rhr-2* did not show enhanced ammonia excretion rates when exposed to a low pH environment,

31 suggesting that RHR-2 represents the apical NH_3 pathway that allows ammonia trapping *via* the

32 hypodermis in N2 worms. A hypothetical model for the mechanism of hypodermal ammonia

33 excretion is proposed on the basis of data in this and previous investigations.

34

35

36

37

38

39 **Keywords:** Rh-proteins, Na^+/K^+-ATPase, V-ATPase, NHX-3, ammonia trapping.

Introduction

Transmembrane transport of ammonia[1], the primary end product of protein catabolism (Campbell, 1991), serves essential physiological functions that include the uptake of nitrogen in animals living on a nitrogen poor diet (Weihrauch, 2006), the adjustment of acid-base homeostasis (Fehsenfeld and Weihrauch, 2012; Weiner and Verlander, 2013) and the excretion of nitrogenous waste in ammonotelic animals, such as fish and aquatic invertebrates (Larsen et al., 2014; Weihrauch et al., 2009; Wright and Wood, 2009). Ammonia exists in a pH-dependent equilibrium of NH_3 and NH_4^+ and occurs predominantly in its ionic form at physiological pH (7.2 - 8), given its pKa of approximately 9.3 (Cameron and Heisler, 1983). Due to its similar size to K^+ ions when hydrated (Weiner and Hamm, 2007), NH_4^+ can serve as a substrate for numerous K^+ transporting proteins and enzymes that includes the Na^+/K^+-ATPase (Cruz et al., 2013; Skou, 1960; Wood et al., 2013), H^+/K^+-ATPase (Swarts et al., 2005), K^+ channels (Choe et al., 2000), and $Na^+/K^+/2Cl^-$ cotransporters (Good et al., 1984). In addition, NH_4^+ may also substitute for alkali metal ions in cation/H^+ exchangers (Blaesse et al., 2010). The gaseous form of ammonia, NH_3, on the other hand, cannot be actively transported across biomembranes, but requires a partial pressure gradient (ΔP_{NH3}) and ideally a NH_3-permeable channel for transmembrane passage. In animals, such NH_3-channels have been identified to be glycosylated proteins belonging to the Rhesus-protein family. These Rh-proteins are well conserved within the animal kingdom (Huang and Peng, 2005) and are predicted to form trimeric complexes *in vivo*, wherein each monomer allows the passage of NH_3 (Gruswitz et al., 2010; Marini et al., 2000). Since their discovery by Marini and coworkers (Marini et al., 2000), numerous studies

---

[1] In the present study "NH_3" refers to gaseous ammonia, "NH_4^+" to the ionic form, and the term "ammonia" is the sum of both molecules.

61 have shown the importance of Rh-proteins in acid-base regulation and epithelial ammonia

62 transport processes, which have been extensively reviewed (Huang and Ye, 2010; Nakhoul and

63 Lee Hamm, 2013; Weihrauch et al., 2009; Weiner and Verlander, 2013; Wright and Wood,

64 2009; Wright et al., 2014). In many ammonia transporting epithelia, including the mammalian

65 distal nephron, fish gills, and anal papillae of dipteran insect larvae, two Rh-proteins are found,

66 one localized on the apical and the other on the basolateral cell membrane, respectively. In a

67 recent study, the ammonia excretion mechanism across the hypodermis of the soil dwelling

68 nematode *C. elegans* was investigated (Adlimoghaddam et al., 2015). As in insects (Weihrauch

69 et al., 2011), *C. elegans* also expresses two Rh-proteins, named RHR-1 and RHR-2. RHR-1 is

70 expressed in many tissues of *C. elegans* but predominantly in the hypodermis (Ji et al., 2006).

71 Moreover, RHR-1 shares high sequence similarity to other vertebrate and invertebrate Rh-

72 proteins and has been shown to function as an ammonia transporter when expressed in yeast

73 (Adlimoghaddam et al., 2015). The latter study also suggested that some ammonia is actively

74 transported from the body fluids *via* the Na^+/K^+-ATPase into the cytoplasm of the hypodermal

75 syncytium. A portion of the cytoplasmic ammonia is then believed to be trapped into acidified

76 vesicles, which are then transported to the apical membrane for exocytotic release

77 (Adlimoghaddam et al., 2015). The lack of transcriptional alterations in response to internal

78 ammonia loading suggested that RHR-1 serves as a housekeeping gene and is likely localized to

79 the basal membrane of the hypodermis (Adlimoghaddam et al., 2015). However, due to its

80 unknown tissue localization and function, the role of the second Rh-protein, RHR-2, in the

81 ammonia transport processes of the worm remains unresolved.

82   Our earlier study suggested an ammonia trapping mechanism across the apical membrane

83   of the hypodermis of the worm (Adlimoghaddam et al., 2015). NH_3 channels in the apical

84   membrane of the hypodermis are thus required for this mechanism to operate.

85   In the current investigation, tissue localization and potential functions of RHR-2 was

86   investigated through the use of transgenic GFP (green fluorescence protein)-constructs as well as

87   transport studies and gene-expression analysis in *rhr-2* knock-out mutant, Δ*rhr-2*.

88   **Material and methods**

89   *Nematode cultures*

90   The hermaphrodite wild-type *Caenorhabditis elegans* strain (N2) and RB651 *rhr-*

91   *2*(*ok403*) knock out worm (Δ*rhr-2*) strain were obtained from the *Caenorhaditis* Genetics Center

92   (CGC, University of Minnesota, Minneapolis) and maintained as described earlier

93   (Adlimoghaddam et al., 2015). Strains were maintained in the laboratory on Nematode Growth

94   Medium (NGM) seeded with *Escherichia coli* OP50 at 16°C according to Brenner (Brenner,

95   1974). After revitalization, worms were washed from the plates with M9 buffer (in mmol l^{-1}: 22

96   KH_2PO_4, 43.5 Na_2HPO_4, 85.54 NaCl, and 3 $MgSO_4$, pH 7) and transferred aseptically into 250

97   mL of liquid medium (S-Basal, in mmol l^{-1}: 43 KH_2PO_4, 5.6 K_2HPO_4, and 97 NaCl, 0.92 citric

98   acid monohydrate, 8.81 tri-potassium citrate monohydrate, 0.048 disodium EDTA, 0.024

99    $FeSO_4.7H_2O$, 0.015 $MnCl_2.4H_2O$, 0.017 $ZnSO_4.7H_2O$, 0.00097 $CuSO_4.5H_2O$, 2.92 $CaCl_2$, and

100   2.92 $MgSO_4$.). The liquid culture medium was enriched with "heat killed" *E. coli* OP50 as a food

101   source and agitated (Innova 2000 platform-shaker, New Brunswick, Canada, RT) at 200 rpm for

102   three days before worms were used in experiments. All experiments on living worms were

103   performed at room temperature (RT, 22 °C). *rhr-2* (*ok403*) is predicted to have most of exon five

104   and all of exons six to nine removed and is the strongest loss-of-function allele available for this

105   gene. Loss of sequence in the mutant strain was verified by PCR (figure S1). For genotypic

106   analysis genomic DNA was extracted from the N2 or *rhr-2* (*ok403*) strains using a single worm

107   lysis protocol. Twenty hermaphrodites were placed in 20 µL of worm lysis buffer (mmol l^{-1} : 50

108   KCl, 2.5 $MgCl_2$, 10 Tris-HCl pH 8.3, 0.45% Tween-20, 0.45% NP40 (IGEPAL), 0.01% gelatin

109   and 1.0 mg/mL of Proteinase K), the worms were freeze thawed or stored at -80°C then

110   incubated at 60°C for 90 minutes and 95°C for 15 minutes. Immediately following lysis 2 µL of

111   the lysate was taken to the PCR reaction.

112   ***Plasmid construction***

113   To create the pJDK4 transcriptional reporter construct *rhr-2p*::GFP, the entire upstream

114   promoter region of *rhr-2* gene, sequences between the stop codon of the upstream gene (*npp-22*)

115   to the ATG start codon of *rhr-2* gene was cloned into the pPD95.77 vector (a gift from Andrew

116   Fire). The pJDK5 translational reporter, *rhr-2*::GFP, includes the above promoter region and the

117   entire *rhr-2* genomic region fused in frame to GFP in the pPD95.77 vector. For pJDK4, the *rhr-*

118   *2* promoter was PCR amplified using forward primers (oJDK9/CeRhr-2 SmaI F:

119   GGGG<u>CCCGGGG</u>AAAATTCATACAACGTTTCCCA; oJDK11/CeRhr-2 AgeI R:

120   GGGG<u>ACCGGTT</u>CTGGAATTTTTCGTAGAAATTTA), and Phusion high-fidelity DNA

121   polymerase (Thermo Scientific, Ottawa, ON, Canada). Further, both PCR fragments and

122   pPD95.77 vector (deletion) were digested with the same FastDigest restriction enzymes

123   (FastDigest kit, Thermo Scientific, Ottawa, Ontario, Canada) overnight at 37°C. The digested

124   products were electrophoresed and purified using the gel extraction kit (QIAquick gel extraction

125   kit, Qiagen Inc, Mississauga, Ontario, Canada). The resulting products were ligated (Promega,

126   Madison, WI, USA) together overnight at 4°C, creating a transcriptional fusion product. Further,

127   the cloned product was transformed into chemically competent *E. coli* DH5α strain and grown in

128   LB containing 100μg/mL ampicillin overnight at 37 °C. At the end of incubation period, colonies

129   were screened by PCR for correct insertion. Vectors containing the *rhr-2* promoter were isolated

130   from the overnight culture using the Qiaprep Spin Miniprep kit (Qiagen, Mississauga, ON,

131   Canada). pJDK5 was created using a three part PCR cloning approach. The promoter and

132   genomic region was amplified from N2 genomic DNA using oJDK9/CeRhr-2 SmaI F:

133   GGGGCCCGGGGAAAATTCATACAACGTTTCCCA and reverse primer oJDK8

134   GAAAAGTTCTTCTCCTTTACTCATATAGATTTCCTGCATTTGCTCA creating a PCR

135   fragment with the stop codon of the *rhr-2* sequence (underlined) removed and fused in frame to

136   the ATG of the GFP protein. The GFP protein was amplified from pPD95.77 using the forward

137   complement of oJDK8, oJDK7

138   TGAGCAAATGCAGGAAATCTATATGAGTAAAGGAGAAGAACTTTTC and a vector

139   specific reverse primer oJDK10 CAAGTTGGTAATGGTAGCGACC. The oJDK8/9 and

140   oJDK7/10 PCR products were run on an agarose gel and gel extracted as above. The two

141   isolated fragments were added in equimolar amounts to a third PCR and amplified using oJDK9

142   and oJDK10 primers. The resulting large PCR fragment and pPD95.77 vector were digested

143   with SmaI and XhoI, gel extracted, ligated and transformed as described above. The fidelity of

144   the pJDK4 transcriptional and pJDK5 translational plasmids were verified by Sanger sequencing

145   (Robarts Research Institute, London, Ontario, Canada).

146   ***Microinjection***

147   The transcriptional construct (40 ng/μL) pJDK4 *rhr-2p*::GFP was co-injected with 40

148   ng/μL pRF4 (*rol-6(su1006)*), and 20 ng/μL pBSII) into the gonads of young adult

149   hermaphrodites (N2). Rolling F1 progeny were selected and stable F2 lines were maintained.

150   The translational reporter pJDK5 *rhr-2*::GFP (90 ng/µL) was co-injected with pJH1774 *myo-*

151   *3p*::mWORMCHERRY (10 ng/µL). Independent F2 transgenic lines were maintained through

152   the selection of body wall muscle specific expression of mWORMCHERRY.

153   Immunohistochemistry and imagining of live transgenics were performed on JDK108 *korEx12*

154   [pJDK5 *rhr-2*::GFP pJH1774 *myo-3p*::mWORMCHERRY].

155   ***Fluorescence microscopy***

156   Animals from stable transgenic lines were placed on slides with 2% agar pads with 10

157   mmol l^{-1} sodium azide or 10 mmol l^{-1} levamisol. The animals transgenic for the transcriptional

158   reporter, *rhr-2p*::GFP, were analyzed with a Zeiss Images A.1 compound microscope. Images

159   were recorded and analyzed with Axiovision software (Zeiss, Toronto, Canada). Larvae and

160   adults transgenic for the translational reporter, *rhr-2*::GFP and *myo-3p*::mWORMCHERRY,

161   were analyzed using the Zeiss LSM700 scanning confocal. Serial z-plane sections were obtained

162   using a 488 nm and 555 nm wavelength optimized emission filter and 585nM and 601nM diode

163   laser to detect the GFP and mWORMCHERRY respectively. Sectioning depth and pinhole

164   diameter (range 33-47 µm and 30-41 µm) were optimized for the objective magnification and

165   detection of the two excitation wavelengths. z-planes of each optical series were processed using

166   maximum z projections using ImageJ.

167   ***Nitrogen excretion experiments***

168   Ammonia excretion rates were determined under the influence of various pH regimes in a

169   series of short-term (2 h) experiments. N2 or Δ*rhr-2* worms (0.1-0.15 g) from liquid culture were

170   washed twice with control medium (in mmol l^{-1}: 22 KCl, 129 NaCl, 1 $MgSO_4$, adjusted to pH 7)

171   followed each time by a centrifugation step (188 x *g*, 1 min at room temperature). After the

172   washing steps, worms were then exposed either to control media adjusted to pH 7, low pH media

173   (control media enriched with 5 mmol l^{-1} 2-(N- orpholino) ethanesulfonic acid (MES), adjusted to

174   pH 5), or high pH media (control media enriched with 5 mmol l^{-1} tris (hydroxymethyl)

175   aminomethane hydrochloride (Tris-HCl), adjusted to pH 8.0) for two hours. During the two hour

176   incubation period, worms were agitated (Innova 2000 platform-shaker, New Brunswick, Canada)

177   at 200 rpm. At the end of the incubation period, worms were pelleted by centrifugation (188 x g,

178   3 min) to determine a fresh worm mass and the collected supernatant of the respective media was

179   immediately frozen at -80 ºC for later analysis of total ammonia and urea concentrations.

180   ***Determination of ammonia and urea by NH$_3$-selective electrode***

181   Ammonia concentration in samples was measured using a gas-selective NH$_3$ electrode

182   (Thermo Orion (ORI9512BNWP), Beverly, USA) connected to a mV/pH meter as described for

183   the previous study on ammonia excretion in *C. elegans*. All media for the standards curves were

184   prepared at the same time with identical composition and pH as the experimental media

185   (Adlimoghaddam et al., 2015).   Urea concentration was measured in an aliquot of the sample

186   treated with 10 unit/ml of urease type II (Sigma, Saint Louis, USA), which catalyzes the

187   conversion of urea to ammonia and bicarbonate. Total ammonia (*i.e.* background plus urea-

188   derived ammonia) was determined after 30 minutes incubation at room temperature. The urea

189   concentration was then determined by subtracting background ammonia (measured in a parallel

190   sample) from total ammonia. The resulting value was then divided by 2 to obtain the urea

191   concentration of the sample. Standard curves were made with the respective experimental

192   solutions, enriched with known concentrations of NH$_4$Cl.

193

194   *Quantitative real-time PCR*

195   RNA was isolated from worms after each experiment described in the figure legends.

196   Total RNA was isolated from N2 and Δ*rhr-2* mutants using the RNeasy plus Mini Kit (Qiagen

197   Inc, Mississauga, Ontario, Canada) under RNase-free conditions. RNA samples were treated

198   with DNase I (Invitrogen, Carlsbad, CA, USA) to remove any genomic DNA contamination. The

199   treated RNA was then tested for genomic DNA by a 40 cycle PCR, employing the primer pair

200   CeActin-F/R primer pair listed in Table 1.

201   Integrity of RNA was checked by both gel electrophoresis and spectrophotometric

202   quantification (Nanodrop 2000C, Nanodrop Technologies, Wilmington, DE, USA).

203   Subsequently, DNase treated total RNA (0.3 µg) was reverse transcribed into cDNA using

204   Superscript II reverse transcriptase and oligo-dT primer (iScript™ cDNA Synthesis Kit, Biorad,

205   Mississauga, Ontario, Canada). The quality of cDNAs was tested before quantitative PCR by

206   standard PCR (CeActin-F/ R) followed by gel electrophoresis and product visualization using

207   ethidium bromide. PCR protocols were optimized for each gene (Table 1) and correctness of the

208   respective PCR products was verified by sequencing (Robarts Research Institute, London,

209   Ontario, Canada).

210   Standard curves for qPCR were generated utilizing a dilution series of known quantities

211   (10^{+3}, 10^{+2}, 10^{+1}, 10^{+0}, 10^{-1} fg DNA) of the respective purified PCR product (QIAquick PCR

212   Purification Kit, Qiagen Inc, Mississauga, Ontario, Canada) of the target gene, with R^2 values $\geq$

213   0.98. All primers, annealing temperatures and PCR product size values are listed in table 1.

214   SSoFast^{TM} EvaGreen supermix (Biorad, Mississauga, Ontario, Canada) and a Biorad

215   MiniOpticon RT-PCR machine (Miniopticon, Biorad, Mississauga, Ontario, Canada) were used

216   for qPCR. Single product amplification was verified at the end of the reaction by means of

217   melting curve analysis.

218   ***Measurements of H+ flux using the scanning ion electrode technique (SIET)***

219   Worms were bathed in moderately hard reconstituted water (MHRW) (Khanna et al.,

220   1997) containing (in mmol l^{-1}): 1 NaCl, 1 $NaHCO_3$, 0.3 $CaCl_2$ and 0.1 KCl. Levamisole (0.5

221   mmol l^{-1}) was added to all media to minimize worm movements during SIET measurements, as

222   described previously (Adlimoghaddam et al., 2014). Net transport of H^+ produced small

223   concentration differences in [H^+] in the unstirred layer next to the surface of the worm. H^+

224   concentration gradients within the unstirred layer near the surface of the worm were determined

225   from measurements of H^+-selective microelectrode voltage using the following equation:

226     $\Delta C = C_B \, 10^{(\Delta V / S)} - C_B$

227   where ΔC is the concentration gradient between the two points (μmol cm^{-3}); C_B is the

228   background H^+ concentration (μmol cm^{-3}), calculated as the average of the concentrations at each

229   point; ΔV is the voltage gradient (μV); and S is the slope of the electrode (μV) for a 10-fold

230   change in ion concentration bracketing the range of interest. The concentration gradient was

231   subsequently converted into an estimate of H^+ flux using Fick's first law of diffusion:

232            $J_{H+} = D_{H+} \, \Delta C / \, \Delta x$

233   where J_{H+} is the net flux of the ion (pmol cm^{-2} s^{-1}), D_{H+} is the H^+ diffusion coefficient (9.31$\times$10^{-}

234   ^{5} cm^2 s^{-1}) and Δx is the distance between the two points measured (cm). H^+ fluxes were corrected

235   for the effects of buffering by H_2O and HCO_3^- using equations published previously (Messerli et

236   al., 2006). SIET methods and H^+-selective microelectrode fabrication and calibration have been

237   described in our earlier paper (Adlimoghaddam et al., 2014). At each site along the hypodermis,

238   fluxes were calculated based on the mean of 3 replicate measurements. For each worm, fluxes

11

239   were measured at 5 or more sites separated by $20 - 25$ µm. A mean value for H^+ flux across the

240   hypodermis of each worm was then calculated from the mean values at each site; n values

241   reported in the results indicate the number of worms.

242   *Enzyme activities*

243   Frozen worms were homogenized in approximately 8 volumes of ice-cold 50 mmol l^{-1}

244   imidazole buffer (pH 7.4 at 20°C) using a ground-glass homogenizer. Homogenates were

245   employed directly for measuring enzyme activities, or frozen (-80ºC) for later determination of

246   protein content. Enzyme assays were performed at 20°C. Cytochrome c oxidase was measured at

247   550 nm with a Agilent Cary 100 spectrophotometer (Mulgrave, Australia) in a medium of 50

248   mmol l^{-1} potassium phosphate buffer (pH 7.0 at 20°C), 0.5% (w/v) sodium dodecyl-maltoside and

249   60 µmol l^{-1} of reduced (equine) cytochrome c. The difference in the rate of absorbance change due

250   to the presence of 1 mmol $^{-1}$ KCN was taken as the rate of cytochrome c oxidase activity. Citrate

251   synthase activity was measured as the difference in the rate of absorbance change at 412 nm

252   between the presence and absence of 1.0 mmol $^{-1}$ oxaloacetate in an assay medium consisting of

253   50 mmol $^{-1}$ imidazole (pH 8.0 at 20°C), 0.5 mmol $^{-1}$, 5,5'-dithiobis-(2-nitrobenzoic acid), 0.1

254   mmol^{-1} acetyl-CoA and 0.2% (v/v) of triton X-100. Protein was measured using the bicinchoninic

255   acid assay in the presence of 0.2 % (w/v) sodium deoxycholate using bovine serum albumin as the

256   protein standard.

257

258   *Chemicals*

259   All chemicals and reagents used in this study were purchased from either Sigma-Aldrich

260   (St. Louis, MO, USA) or Fisher Scientific (Ottawa, Ontario, Canada) unless reported otherwise.

261 *Statistical Analysis*

262   For SIET measurements, n represents the number of individual worms. For other

263 measurements, each n value represents the combined pooled worms with a total mass of ca. 0.1-

264 0.15 g. Results have been reported as mean ± standard error of the mean (SEM). Differences in

265 nitrogen excretion rates, enzymatic activities and absolute mRNA expression patterns between

266 control and treatments were evaluated by unpaired Student's t-tests. One-way analysis of

267 variance (ANOVA) followed by significant difference with Tukey's post-hoc test was used to

268 analyze the data shown in figure 3A. Significance of differences was accepted at $p \leq 0.05$ in all

269 statistical analyses. The statistical method used in each particular experiment is given in the

270 respective figure legends.

271

272   **Results**

273   GFP expression activated by the *rhr-2* promotor indicated that RHR-2 is expressed

274 predominantly in the hypodermis, with additional abundance observed in the ventral nerve cord

275 and body wall muscles (figure 1A). Transgenic animal expressing the RHR-2::GFP fusion

276 protein expressed under its own promoter showed strong GFP expression in the hypodermis of

277 adult *C. elegans* (figure 1B) as well as mid-staged larvae (figure 1C-F). In these transgenic

278 animals the body wall muscle cells express mCHERRY as a transgenic marker. Co-localization

279 of RHR-2::GFP and mCHERRY suggests that RHR-2 is also expressed in the body wall

280 muscles. In *C. elegans*, the striated body wall muscles consist of four rows of muscle fibers

281 (Altun and Hall, 2009b). Two rows juxtapose the ventral nerve cord and two juxtapose the

282 dorsal nerve cord. The muscle cells directly contact the hypodermis in these regions. Therefore

283   the lateral regions of the hypodermis is where the subcellular localization of the RHR-2::GFP

284   protein is localized. In figure 1E and F optical sections through the medial-lateral aspects of

285   hypodermis the larvae can be seen. Sections through the large nuclei of the hypodermis (figure

286   1E) show RHR-2::GFP expression in the perinuclear space of the cell as well as concentration at

287   the apical surface. In optical sections where the hypodermis is in contact with the body wall

288   muscle, basolateral expression of the RHR-2::GFP protein in the hypodermis cannot be clearly

289   distinguished. The hypodermis of *C. elegans* is a multinucleate syncytium (Altun and Hall,

290   2009a) with adherens junctions located only at the lateral seam cells. This small area of non-

291   RHR-2::GFP expressing hypodermal cells (figure 1B) make the use of apical junction markers

292   technically difficult.

293

294   To evaluate whether the hypodermal expressed Rh-proteins, RHR-1 and RHR-2, are

295   involved in chronic acid-base regulation, gene-expression levels were monitored in animals

296   acclimated for 2 days to either pH 5.5 or pH 8. Messenger RNA expression levels of *rhr-1*, *rhr-*

297   *2*, as well of the *vat* (subunit A) did not change in either pH when compared to control values

298   (animals acclimated to pH 7 (non-buffered)). A slight up-regulation in mRNA expression was

299   observed only for the *nka* (α-subunit) after a two-day acclimation to pH 8 (figure 2). Absolute

300   gene expression values are provided in the supplemental table S1.

301

302   **The Δ*rhr-2* mutant**

303   There were no noticeable differences between the N2 phenotype and the Δ*rhr-2* mutant

304   (Ji et al., 2006), with the exception found in the current study that adult Δ*rhr-2* mutants tend to

305   be smaller (max. 0.9 mm) compared to N2 worms (1.12-1.15 mm).

306   To assess whether RHR-2 is involved in nitrogen excretion, the *rhr-2* knock-out mutant

307   strain (Δ*rhr-2*) was employed. In comparison to ammonia excretion values measured in fed N2

308   worms in a previous study (Adlimoghaddam et al., 2015), ammonia excretion rates were

309   approximately 82% lower in fed Δ*rhr-2* worms, whereas corresponding urea excretion rates

310   were 95% lower in the mutant (figure 3A, 3B).

311   To further characterize the Δ*rhr-2* strain, hypodermal H^+ fluxes across the hypodermis

312   were measured using SIET. As seen in figure 4, compared to N2, hypodermal H^+ efflux was

313   reduced in Δ*rhr-2* by about 50% (n = 5).

314   During the ammonia and H^+ efflux experiments the worms began in the fed state and thus

315   the majority of excretion will likely reflect dietary intake and excess or acid formation as a result

316   of metabolism. Therefore, taking the assumed balance between nutrient intake and deposition in

317   tissues or excretion the reduction in ammonia and H^+ efflux rates in the Δ*rhr-2* mutant relative to

318   N2 worms could have been a consequence of decreased nutrient intake that reflects a general

319   reduction in metabolic rate. To investigate this possibility, enzyme activity measurements on

320   cytochrome c oxidase and citrate synthase were conducted in fed control N2 worms and the

321   Δ*rhr-2* strain. As shown in figure 5, the activity of cytochrome c oxidase was reduced by more

322   than 50%, consistent with lower maximal mitochondrial respiratory capacity and possibly lower

323   aerobic metabolic activity. However, the activity of citrate synthase showed no difference

324   between N2 and the Δ*rhr-2* strain. The lack of change in citrate synthase activity may reflect the

325   multifaceted role of the Krebs cycle, including both the supply of electrons for oxidative

326   phosphorylation as well as anaplerosis of carbon intermediates during growth. Future metabolic

327   characterization of the Δ*rhr-2* strain should be considered to further address the biochemical

328   impact of losing the RHR-2 protein function.

329   The Δ*rhr-2* strain still exhibited detectable ammonia excretion, albeit at reduced rates. To

330   test whether the hypodermal ammonia trapping described in N2 worms (Adlimoghaddam et al.,

331   2015) also occurred in the mutants, Δ*rhr-2* worms were exposed to an environmental pH of 5.

332   The results showed that ammonia excretion rates remained unaltered under reduced pH. In

333   contrast, when Δ*rhr-2* worms were exposed to pH 8.5, ammonia excretion rates decreased by

334   approximately 45% (figure 3A).

335   The importance of RHR-2 in ammonia transport was further investigated by

336   monitoring changes of expression levels of genes known to be involved in the process. As figure

337   6 shows, mRNA expression levels of *rhr-1*, *nka*, *vat* and *nhx-3* were higher in fed Δ*rhr-2* when

338   compared to fed N2 worms. Only the housekeeping sodium-hydrogen exchanger, *nhx-4*, showed

339   a minor down-regulation in the Δ*rhr-2* strain. Moreover, internal ammonia loads due to feeding

340   caused a substantial up-regulation of *rhr-1*, *nka*, *vat*, *nhx-3* and *nhx-4* in the Δ*rhr-2* strain, when

341   compared to starved animals (figure 7). Absolute gene expression values for these experiments

342   are provided in the supplemental table S2 and S3, respectively.

343

Discussion

345   This paper examined the role of RHR-2 in hypodermal ammonia excretion in *C. elegans*.

346   As shown in figure S1, RHR-2 shares a high level of sequence homology (44% identity in amino

347   acid sequence) to the functionally characterized RHR-1 ammonia transporter in *C. elegans* and

348   contains, in common with RHR-1 and other ammonia transporting Rh-proteins, the conserved

349   amino acid residues crucial for ammonia conductance (Adlimoghaddam et al., 2015; Zidi-

350   Yahiaoui et al., 2009). Accordingly, an NH_3 transport function is strongly suggested also for

351   RHR-2. An earlier study revealed that mRNA expression levels of *rhr-2*, but not *rhr-1*, were up-

352   regulated in response to internal ammonia loads after feeding, suggesting an important role of

353   RHR-2 in ammonia excretion processes (Adlimoghaddam et al., 2015). Indeed, expression *rhr-2*

354   promotor activated GFP and the subcellular localization *rhr-2*::GFP translational fusion protein

355   clearly showed that RHR-2 is strongly expressed in the hypodermis (figure 1), underpinning its

356   potential function in hypodermal ammonia excretion.

357   Localization a RHR-2::GFP fusion protein was verified in the apical membrane of the

358   hypodermis in transgenic animals expressing RHR-2::GFP protein worms (figure 1F). The

359   RHR-2::GFP is also detected in the four quadrants of body wall muscles underlying the

360   hypodermis in the larval and adult stages (Figure 1A, B and C). The function of RHR-2

361   expression in the muscle tissue is unknown but a basal location of the protein in the regions

362   where the hypodermis and muscle cells come into direct contact was not optically discernable

363   and therefore is also possible in these regions of the hypodermis. In addition to an apical

364   localization a RHR-2::GFP is associated with the periphery of the nucleus. Further studies on

365   the subcellular localization of the RHR-2 protein may clarify the potential for trafficking of the

366   receptor from the Golgi apparatus to the apical surface of the hypodermal cells.

367   *rhr-2* showed an mRNA up-regulation after feeding or after the exposure to high

368   environmental ammonia (HEA) (Adlimoghaddam et al., 2015) similar to the apically localized

369   Rhcg-2 in the gill epithelia of freshwater rainbow trout (Zimmer et al., 2010). Also, in contrast to

370   N2 worms, which showed increased ammonia excretion rates when exposed to pH 5, likely due

371   to apical ammonia trapping (Adlimoghaddam et al., 2015), ammonia excretion rates in the Δ*rhr-*

372   *2* strain remained unchanged in a low pH environment (figure 3A). This result could well be

373   explained by a missing NH_3 pathway, possibly RHR-2, in the apical membrane of the

374   hypodermis. In addition, mRNA expression levels of *rhr-2* are *ca.* 10 times lower overall, in

17

375   comparison to *rhr-1* (Adlimoghaddam et al., 2015). A similar reduction in expression levels of ~

376   10-fold was also found in the skin of *Xenopus laevis* for Rhcg, when compared to Rhbg (Cruz et

377   al., 2013) and in the skin of the Magadi tilapia *Alcolapia graham* (Rhbg vs. Rhcg1) (Wood et al.,

378   2013). Although not shown for the frog skin specifically, in vertebrate species Rhbg is usually

379   localized to the basolateral membrane of epithelial cells (Han et al., 2013; Verlander et al., 2003;

380   Weihrauch et al., 2009; Wright and Wood, 2009).

381   Interestingly, mRNA expression levels of both *rhr-1* and *rhr-2* did not change

382   significantly when animals were exposed chronically to pH 5.5 or pH 8.

383   This might imply that both Rh-proteins are not substantially involved in the regulation of

384   acid or base homeostasis. However, the Rh-protein substrates ammonia and possibly CO2 can be

385   considered as acid-base equivalents and accordingly, a putative role of RHR-1 and RHR-2 in

386   acid-base homeostasis is possible. Likewise, it is possible that the constitutive abundance of the

387   actual transporter proteins is sufficient to maintain their regular function also in the face of

388   changing environmental pH conditions.

389

390   Moreover, as predicted for RHR-2, Rhcg-2 in trout gills is also apically localized and its mRNA

391   expression levels do not change significantly when fish are exposed for 2 days to an alkaline pH

392   (Sashaw et al., 2010), implying again a similar localization and role of these two Rh-proteins in

393   the ammonia excretion process.

394   The lack of response seen for *rhr-1* and *rhr-2* mRNA expression under the influence of

395   low and high environmental pH regimes stands in contrast to our recent observation investigating

396   epithelial cation/proton exchangers in *C. elegans*. In response to exposure to pH 5.5 and 8, a

397   significant up-regulation of mRNA for *nhx-3* in the hypodermis and *nhx-2* in the apical

398   membrane of the intestine was observed, and a concomitant down-regulation of *nhx-9*, expressed

399   in the excretory cell (Adlimoghaddam pers. communication). This is an indication that the NHEs

400   in *C. elegans* are key players in cellular and organismal acid-base homeostasis, as shown for

401   many other animal systems (Orlowski and Grinstein, 2004; Zachos et al., 2005).

402

403   **The Δ*rhr-2* mutant as a system to investigate the role of RHR-2 in ammonia transport**

404   The Δ*rhr-2* strain used in our studies is predicted to remove or disrupt function in seven

405   of the eight highly conserved amino acid residues predicted to be required for RHR-2 pore

406   formation and specific interaction with the ammonia molecule (figure S1). Our results indicate

407   that protein metabolism in the Δ*rhr-2* strain was compromised or slowed, as evident from the

408   reductions in the rates of ammonia excretion and hypodermal H^+ excretion, as well as from the

409   lower specific activity of cytochrome c oxidase. On the other hand the mutant revealed no drastic

410   changes in its phenotype, except for a slightly shorter body length.

411   In fact, experiments employing the Δ*rhr-2* mutant strain provided useful information regarding

412   the role of Δ*rhr-2* in the ammonia excretion processes in *C. elegans*. Mutant worms showed an

413   up-regulation of *rhr-1*, *nka* (α-subunit) and *vat* (subunit A), transcripts of transporters known to

414   be involved in the ammonia excretion mechanism in *C. elegans* (figure 6) (Adlimoghaddam et

415   al., 2015). We suggest that up-regulation of these transporters is a compensatory response to the

416   lack of the hypodermal ammonia transporter, as is the increase in mRNA levels for hypodermal-

417   expressed *nhx-3*. NHX-3 is localized in intracellular plasma membrane vesicles (Nehrke and

418   Melvin, 2002) and was also up-regulated in N2 worms after an internal ammonia load due to

419   feeding (Adlimoghaddam per. communication). NHX-4 is ubiquitously expressed and targeted to

420   the basolateral membrane, and likely functions as a housekeeping gene, similar to the

421 mammalian NHE-1 (Nehrke and Melvin, 2002). The observed down-regulation of *nhx-4* in the

422 mutant may thus be explained by the reduction in metabolism in the Δ*rhr-2* strain relative to N2

423 worms. Note, it must be mentioned that changes of the gene transcripts were significant but

424 rather small. A follow-up study employing custom made antibodies must verify that

425 corresponding proteins show indeed changes in abundance.

426   When starved Δ*rhr-2* mutant worms were refed, all investigated transporter genes showed

427 a strong up-regulation on the transcript level (figure 7). The observed up-regulation of these

428 genes was several times higher than that seen in earlier studies of fed N2 worms

429 (Adlimoghaddam et al., 2015). Importantly, while mRNA expression levels of *rhr-1* in N2

430 worms were unaffected by feeding, feeding of Δ*rhr-2* mutants caused a more than 12-fold up-

431 regulation of *rhr-1* mRNA, underpinning a possibly greater importance for this protein when the

432 second hypodermal ammonia transporter, RHR-2, is lacking. In turn, this result emphasizes the

433 overall importance of RHR-2 in excretion of ammonia across the hypodermis.

434

435 **Conclusion**

436   Our data indicate a central role for RHR-2 in hypodermal ammonia excretion and suggest

437 strongly that RHR-2 resides in the apical of this tissue and possibly also in the basolateral

438 membrane. Moreover, experiments employing the Δ*rhr-2* mutant verified the importance of

439 other transporters, such as RHR-1, Na^+/K^+-ATPase, V-ATPase and NHX-3 in ammonia

440 excretion, as suggested also in earlier studies. A working model for the hypodermal ammonia

441 excretion mechanisms incorporates findings from both, this current study and previous work on

442 *C. elegans* (Adlimoghaddam et al., 2015) (figure 8). The hypothetical model proposes that NH_4^+

443 from the body fluids enters the hypodermis *via* the $Na^+/K^+ (NH_4^+)$-ATPase, as the enzyme

444   accepts also NH_4^+ as a substrate (Adlimoghaddam et al., 2015). In addition, NH_3 may also enter

445   *via* RHR-1 and/or RHR-2 on the basolateral membrane, depending on the prevailing ΔP_{NH3}. It is

446   likely that the Rh-proteins also serve as entrance pathways for CO_2, based on studies of Rhesus

447   protein function in other animals (Endeward et al., 2008; Kustu and Inwood, 2006; Perry et al.,

448   2010). Intracellular ammonia occurs in a pH-dependent equilibrium of NH_4^+ and $NH_3 + H^+$.

449   Protons produced by the action of carbonic anhydrase are transported *via* an apically localized

450   V-ATPase into the multilayered cuticle (unstirred boundary layer)(Peixoto and De Souza, 1995),

451   thereby generating a partial pressure gradient for NH_3 (ΔP_{NH3}). According to the current study,

452   some NH_3 follows the ΔP_{NH3} *via* the apically localized RHR-2 and is trapped outside as NH_4^+.

453   In addition to this mechanism, NH_3 may follow ΔP_{NH3} into intracellular vesicles that are acidified

454   by NHX-3 and/or a V-ATPase. Whether NH_3 crosses the vesicular membrane *via* simple

455   diffusion or also *via* an NH_3-channel awaits further investigations. As excretion was inhibited by

456   colchicine (Adlimoghaddam et al., 2015) it is further suggested that the NH_4^+ laden vesicles are

457   then transported along the microtubule network to the apical membrane, where NH_4^+ is released

458   by exocytosis.

459   An intriguing aspect of the hypothesized hypodermal ammonia excretion mechanism in

460   *C. elegans* is its dual nature; the model incorporates both the apical ammonia trapping

461   mechanisms found in the transporting epithelia of freshwater organisms, such as the trout gill

462   (Wright and Wood, 2009) or the body surface of planarians and leeches (Quijada-Rodriguez et

463   al., 2015; Weihrauch et al., 2012), as well as the vesicular transport of ammonia found in

464   brackish/seawater water dwelling invertebrates, as described for the gills of the green crab

465   *Carcinus maenas* (Weihrauch et al., 2002). The nematode's habitat (soil) might indeed demand

466   physiological adaptations that have led to a co-existence of the two excretory mechanisms.

467   Sodium concentrations of the water film around soil particles can be quite low (< 6 mmol kg^{-1})

468   (Haynes and Williams, 1992), and, as a consequence, an active secretion of cations (protons)

469   may be required to hyperpolarize the apical membrane in order to drive Na$^+$ uptake from a Na$^+$-

470   poor environment. Such a mechanism is commonly found in the osmoregulatory epithelia of

471   freshwater species (Larsen et al., 2014). Apical secretion of H$^+$, as shown for the hypodermis of

472   *C. elegans*, will also create a ΔP_{NH_3} and promote apical ammonia excretion. To function to its

473   fullest extent, this apical ammonia trapping mechanism requires a "strong" unstirred boundary

474   layer, where proton gradients could be sustained and therefore consequently also an environment

475   with low buffer capacity. Compared to freshwater, however, soil may have a very high buffer

476   capacity (Federer and Hornbeck, 1984). Vesicular transport, as found in gills of marine

477   crustaceans, may thus be advantageous for soil nematodes since it provides an additional

478   ammonia excretion mechanism that is relatively independent of environmental pH.

479

480

485

486

487

488

489

22

490

491

492

Literature

Adlimoghaddam, A., Boeckstaens, M., Marini, A.M., Treberg, J.R., Brassinga, A.-K., Weihrauch, D., 2015. Ammonia excretion in *Caenorhabditis elegans*: mechanism and evidence of ammonia transport of the Rh-protein CeRhr-1. J Exp Biol 218, 675-683.

Adlimoghaddam, A., Weihrauch, D., O'Donnell, M.J., 2014. Localization of K^+, H^+, Na^+ and Ca^{2+} fluxes to the excretory pore in *Caenorhabditis elegans*: application of scanning ion-selective microelectrodes. The Journal of experimental biology 217, 4119-4122.

Altun, Z.F., Hall, D.H., 2009a. Epithelial system, hypodermis., WormAtlas.

Altun, Z.F., Hall, D.H., 2009b. Muscle system, somatic muscle., WormAtlas.

Blaesse, A.K., Broehan, G., Meyer, H., Merzendorfer, H., Weihrauch, D., 2010. Ammonia uptake in Manduca sexta midgut is mediated by an amiloride sensitive cation/proton exchanger: Transport studies and mRNA expression analysis of NHE7, 9, NHE8, and V-ATPase (subunit D). Comp Biochem Physiol A Mol Integr Physiol 157, 364-376.

Brenner, S., 1974. The genetics of Caenorhabditis elegans. Genetics 77, 71-94.

Cameron, J.N., Heisler, N., 1983. Studies of ammonia in the rainbow trout: Physicochemical parameters, acid-base behaviour and respiratory clearance. J Exp Biol 105, 107-125.

Campbell, J.W., 1991. Excretory nitrogen metabolism, in: C.L. Prosser (Ed.), Environmental and Metabolic Animal Physiology. Wiley, New York, 277-324.

Choe, H., Sackin, H., Palmer, L.G., 2000. Permeation properties of inward-rectifier potassium channels and their molecular determinants. J Gen Physiol 115, 391-404.

Cruz, M.J., Sourial, M.M., Treberg, J.R., Fehsenfeld, S., Adlimoghaddam, A., Weihrauch, D., 2013. Cutaneous nitrogen excretion in the African clawed frog Xenopus laevis: effects of high environmental ammonia (HEA). Aquat Toxicol 136-137, 1-12.

Endeward, V., Cartron, J.P., Ripoche, P., Gros, G., 2008. RhAG protein of the Rhesus complex is a CO2 channel in the human red cell membrane. FASEB J 22, 64-73.

Federer, C.A., Hornbeck, J.W., 1984. The buffer capacity of forest soils in New England. Water, Air, and Soil Pollution 26, 163-173.

Fehsenfeld, S., Weihrauch, D., 2012. Differential acid-base regulation in various gills of the green crab *Carcinus maenas*: Effects of elevated environmental pCO2. . Com Biochem Physiol. A Submitted, ms. 21318

Good, D.W., Knepper, M.A., Burg, M.B., 1984. Ammonia and bicarbonate transport by thick ascending limb of rat kidney. Am J Physiol 247, F35-44.

Gruswitz, F., Chaudharya, S., Ho, J.D., Schlessinger, A., Pezeshki, B., Ho, C.-M., Sali, A., M., W.C., Stroud, R.M., 2010. Function of human Rh based on structure of RhCG at 2.1 Å. Proc Natl Acad Sci U S A 107, 9638-9643.

Han, K.H., Lee, H.W., Handlogten, M.E., Whitehill, F., Osis, G., Croker, B.P., Clapp, W.L., Verlander, J.W., Weiner, I.D., 2013. Expression of the ammonia transporter family member, Rh B Glycoprotein, in the human kidney. Am J Physiol Renal Physiol 304, F972-981.

531 Haynes, R.J., Williams, P.H., 1992. Changes in soil solution composition and pH in urine-
532 affected areas of pasture. Journal of Soil Science 43, 323-334.
533 Huang, C.H., Peng, J., 2005. Evolutionary conservation and diversification of Rh family genes
534 and proteins. Proc Natl Acad Sci U S A 102, 15512-15517.
535 Huang, C.H., Ye, M., 2010. The Rh protein family: gene evolution, membrane biology, and
536 disease association. Cell Mol Life Sci 67, 1203-1218.
537 Ji, Q., Hashmi, S., Liu, Z., Zhang, J., Chen, Y., Huang, C.H., 2006. CeRh1 (rhr-1) is a dominant
538 Rhesus gene essential for embryonic development and hypodermal function in Caenorhabditis
539 elegans. Proc Natl Acad Sci U S A 103, 5881-5886.
540 Khanna, N., Cressman III, C., Tatara, C., Williams, P., 1997. Tolerance of the nematode
541 *Caenorhabditis elegans* to pH, salinity, and hardness in aquatic media. Archives of
542 environmental contamination and toxicology 32, 110-114.
543 Kustu, S., Inwood, W., 2006. Biological gas channels for NH3 and CO2: evidence that Rh
544 (Rhesus) proteins are CO2 channels. Transfus Clin Biol 13, 103-110.
545 Larsen, E.H., Deaton, L.E., Onken, H., O'Donnell, M., Grosell, M., Dantzler, W.H., Weihrauch,
546 D., 2014. Osmoregulation and excretion. Comprehensive Physiology 4, 405-573.
547 Marini, A.M., Matassi, G., Raynal, V., Andre, B., Cartron, J.P., Cherif-Zahar, B., 2000. The
548 human Rhesus-associated RhAG protein and a kidney homologue promote ammonium transport
549 in yeast. Nat Genet 26, 341-344.
550 Messerli, M.A., Robinson, K.R., Smith, P.J., 2006. Electrochemical sensor applications to the
551 study of molecular physiology and analyte flux in plants, Plant Electrophysiology. Springer, 73-
552 107.
553 Nakhoul, N.L., Lee Hamm, L., 2013. Characteristics of mammalian Rh glycoproteins (SLC42
554 transporters) and their role in acid-base transport. Molecular aspects of medicine 34, 629-637.
555 Nehrke, K., Melvin, J.E., 2002. The NHX family of Na+-H+ exchangers in Caenorhabditis
556 elegans. J Biol Chem 277, 29036-29044.
557 Orlowski, J., Grinstein, S., 2004. Diversity of the mammalian sodium/proton exchanger SLC9
558 gene family. Pflugers Arch 447, 549-565.
559 Peixoto, C.A., De Souza, W., 1995. Freeze-fracture and deep-etched view of the cuticle of
560 Caenorhabditis elegans. Tissue Cell 27, 561-568.
561 Perry, S.F., Braun, M.H., Noland, M., Dawdy, J., Walsh, P.J., 2010. Do zebrafish Rh proteins act
562 as dual ammonia-CO2 channels? J Exp Zool A Ecol Genet Physiol 313, 618-621.
563 Quijada-Rodriguez, A.R., Treberg, J.R., Weihrauch, D., 2015. Mechanism of ammonia excretion
564 in the freshwater leech Nephelopsis obscura: characterization of a primitive Rh protein and
565 effects of high environmental ammonia. Am J Physiol Regul Integr Comp Physiol 309, R692-
566 705.
567 Sashaw, J., Nawata, M., Thompson, S., Wood, C.M., Wright, P.A., 2010. Rhesus glycoprotein
568 and urea transporter genes in rainbow trout embryos are upregulated in response to alkaline
569 water (pH 9.7) but not elevated water ammonia. Aquat Toxicol 96, 308-313.
570 Skou, J.C., 1960. Further investigations on a Mg^{++} + Na^+-activated adenosinetriphosphatase,
571 possibly related to the active, linked transport of Na+ and K+ across the nerve membrane. .
572 *Biochim Biophys Acta* 42, 6-23.
573 Swarts, H.G., Koenderink, J.B., Willems, P.H., De Pont, J.J., 2005. The non-gastric H,K-ATPase
574 is oligomycin-sensitive and can function as an H+,NH4(+)-ATPase. J Biol Chem 280, 33115-
575 33122.

576 Verlander, J.W., Miller, R.T., Frank, A.E., Royaux, I.E., Kim, Y.H., Weiner, I.D., 2003.
577 Localization of the ammonium transporter proteins RhBG and RhCG in mouse kidney. Am J
578 Physiol Renal Physiol 284, F323-337.
579 Weihrauch, D., 2006. Active ammonia absorption in the midgut of the Tobacco hornworm
580 Manduca sexta L.: Transport studies and mRNA expression analysis of a Rhesus-like ammonia
581 transporter. Insect Biochem Mol Biol 36, 808-821.
582 Weihrauch, D., Chan, A.C., Meyer, H., Doring, C., Sourial, M.M., O'Donnell, M.J., 2012.
583 Ammonia excretion in the freshwater planarian Schmidtea mediterranea. J Exp Biol 215, 3242-
584 3253.
585 Weihrauch, D., Donini, A., O'Donnell, M.J., 2011. Ammonia transport by terrestrial and aquatic
586 insects. J Insect Physiol 58, 473-487.
587 Weihrauch, D., Wilkie, M.P., Walsh, P.J., 2009. Ammonia and urea transporters in gills of fish
588 and aquatic crustaceans. J Exp Biol 212, 1716-1730.
589 Weihrauch, D., Ziegler, A., Siebers, D., Towle, D.W., 2002. Active ammonia excretion across
590 the gills of the green shore crab *Carcinus maenas*: participation of $Na(+)/K(+)$-ATPase, V-type
591 $H(+)$-ATPase and functional microtubules. J Exp Biol 205, 2765-2775.
592 Weiner, I.D., Hamm, L.L., 2007. Molecular mechanisms of renal ammonia transport. Annu Rev
593 Physiol 69, 317-340.
594 Weiner, I.D., Verlander, J.W., 2013. Renal ammonia metabolism and transport. Comprehensive
595 Physiology 3, 201-220.
596 Wood, C.M., Nawata, C.M., Wilson, J.M., Laurent, P., Chevalier, C., Bergman, H.L., Bianchini,
597 A., Maina, J.N., Johannsson, O.E., Bianchini, L.F., Kavembe, G.D., Papah, M.B., Ojoo, R.O.,
598 2013. Rh proteins and $NH4(+)$-activated Na+-ATPase in the Magadi tilapia (Alcolapia grahami),
599 a 100% ureotelic teleost fish. J Exp Biol 216, 2998-3007.
600 Wright, P.A., Wood, C.M., 2009. A new paradigm for ammonia excretion in aquatic animals:
601 role of Rhesus (Rh) glycoproteins. J Exp Biol 212, 2303-2312.
602 Wright, P.A., Wood, C.M., Wilson, J.M., 2014. Rh versus pH: the role of Rhesus glycoproteins
603 in renal ammonia excretion during metabolic acidosis in a freshwater teleost fish. J Exp Biol
604 217, 2855-2865.
605 Zachos, N.C., Tse, M., Donowitz, M., 2005. Molecular physiology of intestinal Na+/H+
606 exchange. Annu Rev Physiol 67, 411-443.
607 Zidi-Yahiaoui, N., Callebaut, I., Genetet, S., Le Van Kim, C., Cartron, J.P., Colin, Y., Ripoche,
608 P., Mouro-Chanteloup, I., 2009. Functional analysis of human RhCG: comparison with E. coli
609 ammonium transporter reveals similarities in the pore and differences in the vestibule. Am J
610 Physiol Cell Physiol 297, C537-547.
611 Zimmer, A.M., Nawata, C.M., Wood, C.M., 2010. Physiological and molecular analysis of the
612 interactive effects of feeding and high environmental ammonia on branchial ammonia excretion
613 and Na+ uptake in freshwater rainbow trout. J Comp Physiol B 180, 1191-1204.

614

615

616

617

618

619

620

621

622

623

624   Table 1: Primers employed in qPCR targeting actin, Rhesus (Rh)-like ammonia transporter (*rhr-*

625   *1, rhr-2*), *vat* (subunit A), *nka* (α-subunit), *nhx-3* and *nxh-4* from the nematode *Caenorhabditis*

626   *elegans*.

627

Primer	Nucleotide sequence (5' → 3')	Annealing Temp. (ºC)	Product size (bp)	GenBank Acc. #
Actin				
CeActin-F	ATCGTCCTCGACTCTGGAGAT	60		
CeActin-R	TCACGTCCAGCCAAGTCAAG	60	100	NM_073417
Rhr-1				
CeRhr-1 F	TTCTTGTCTGAGAAACTCGGA	60		
CeRhr-1 R	GATTGCCATAAGCTGGTTCAA	60	210	NM_072035
Rhr-2				
CeRhr-2 F	ACAGTGGTAGATCTCTTTCC	60		
CeRhr-2 R	CGTGCATCTTCTGGTTCTTG	60	205	NM_073560
Na$^+$/K$^+$-ATPase				
CeNKA F	GACCTCGGAACTGACATGGT	60		
CeNKA R	CCCATAAGCAAGGGAGATCA	60	135	U18546
H$^+$-ATPase				
CeVHA F	CTTGAAGGCTCGTGAAGACC	60		
CeVHA R	ACGACTTCCTTTTCGAGCAA	60	150	NM_068639

628

629

630

631

632

633

634 Table S1: Absolute mRNA expression values for *rhr-1*, *rhr-2*, *nka* (α-subunit) and *vat* (subunit
635 A) in *C. elegans* (N2) starved for 24 hours. The values in brackets represent the numbers of
636 biological replicates.

		rhr-1	*rhr-2*	*nka*	*vat* 637
		(fg cDNA ng^{-1} total RNA)			
N2	X	6.4 (5)	0.19 (5)	69.1 (5)	44.4 (5) 638
	SEM	0.5	0.03	5.3	3.7
pH 5.5	X	6.0 (5)	0.24 (4)	65.3 (5)	52.2 (5) 639
	SEM	0.2	0.038	7	3.5
pH 8	X	7.5 (4)	0.2 (5)	95.6 (5)	50.8 (4) 640
	SEM	0.9	0.02	9.5	4.8

641

642

643

644

645

646

647

648

649

650

651

652

653

654

655

656

Table S2: Absolute mRNA expression values for *rhr-1*, *nka* (α-subunit) and *vat* (subunit A), *nhx-3* and *nhx-4* in fed *C. elegans* (N2) and *rhr-2* knock-out mutants, Δ*rhr-2*. Data correspond to figure 6. The values in brackets represent the numbers of biological replicates.

		rhr-1	*nka*	*vat*	*nhx-3*	*nhx-4*
		(fg cDNA ng^{-1} total RNA)				
N2	X	36.1 (4)	375 (4)	262.8 (3)	1.1 (3)	35.6 (5)
	SEM	2.2	9.5	1.1	0.13	2
Δ*rhr-2*	X	49.1 (4)	682.2 (4)	482.0 (4)	2.4 (4)	22.8 (4)
	SEM	3.2	26.0	15.2	0.16	2.0

681 Table S3: Absolute mRNA expression values for *rhr-1*, *nka* (α-subunit) and *vat* (subunit A), *nhx-*
682 *3* and *nhx-4* in fed and starved (24 hours) Δ*rhr-2*. Data correspond to figure 7. The values in
683 brackets represent the numbers of biological replicates.

684

685

		rhr-2	*nka*	*vat*	*nhx-3*	*nhx-4*
		(fg cDNA ng^{-1} total RNA)				
Δ*rhr-2*	X	49.1 (4)	682.2 (4)	482.0 (4)	2.4 (4)	22.8 (4)
	SEM	3.2	26.0	15.2	0.16	2.0
Δ*rhr-2* (starved)	X	3.8 (4)	23.4 (4)	111.0 (4)	0.17 (4)	3.0 (4)
	SEM	0.8	4.5	21.4	0.03	0.9

686

687

688

689

690

691

692

693

694

695

696

697

698

699

700

701

702

703

704

Figure legends:

706

707   Figure 1: A) Adult transgenic *C. elegans* with *rhr-2* promotor activated GFP expression. GFP

708   expression is observed in the hypodermis and ventral nerve cord (white arrow head). Head is

709   oriented to the left. Scale bar = 50 µm. B-F) Transgenic *C. elegans* expressing *rhr-2* promoter

710   driven RHR-2::GFP protein (green) and muscle-specific *myo-3* promoter activated mCHERRY

711   (red). (B) Left lateral surface of young adult shows strong RHR-2::GFP expression in the

712   surface. Head is to the left. Body wall muscles also express RHR-2::GFP, as detected by co-

713   expression of mCHERRY, as well as the spermathecal, vulva, ventral nerve cord and a subset of

714   head neurons. Scale bar 50 µm. Bottom Left: detail of hypodermal RHR-2::GFP expression (200

715   µm in width). RHR-2 is detected in the dorsal and ventral hypodermal cells. Protein is absent

716   from lateral seam cells (open arrow head). C) Dorsal view of a mid-staged larvae expressing

717   RHR-2::GFP and myo-3p::mCHERRY. RHR-2::GFP is detected in the hypodermis, body wall

718   muscle and two head neurons (white arrow head). Scale bar 20 µm. D-F) Serial optical sections

719   through the dors al-ventral plane of a mid-staged larvae. Scale bar 10 µm D) z-projection of

720   serial optical sections of the left lateral aspect of the worm (depth 5.43 µm). RHR-2::GFP is

721   detectable in the dorsal muscle cells and hypodermis (open arrows). E) z-projection of RHR-

722   2::GFP expressing tissues below the muscle cells 1.55 µm in depth. The central intestine of the

723   larvae is visible. RHR-2::GFP expression is obvious in the hypodermis (open arrows). F) 43 µm

724   by 18 µm detail. z-projection of single cells 0.78 µm depth. Apical surface of the hypodermis is

725   facing the top of the figure. The large nuclei of two of the hypodermal cells can be seen

726   (asterisks). RHR-2::GFP can been seen concentrated at the apical surface (open arrow heads) as

727   well as surrounding the nuclei of the hypodermal cells.

728

729   Figure 2: Changes of mRNA expression levels of *rhr-1* (n=4-5), *rhr-2* (n=5), *nka* (α-subunit)

730   (n=4-5) and *vat* (subunit A) (n=4-5) in *C. elegans* after a 2 day exposure to pH 5.5 (A) and pH

731   8.0 (B). Absolute mRNA expression levels of control animals exposed to a non-buffered saline

732   (pH 7) were set to 1 and are indicated by the dotted line. All groups were starved for 24 hours

733   before RNA isolation. The asterisk (*) indicates significant differences between treatments and

734   respective controls ($p \leq 0.05$). Data represent means ± SEM and were analyzed employing an

735   unpaired, two-tailed Student's t-test prior to calculation for fold change values.

736

737   Figure 3: Ammonia (A) and urea (B) excretion rates in wild type (N2) and Δ*rhr-2 C. elegans*.

738   Ammonia excretion rates (n=31) and urea excretion rates (n=4) are represented by black bars

739   (Adlimoghaddam et al., 2015). The asterisks (*) indicate significant differences between N2 and

740   Δ*rhr-2* (open bars, n=4-6) under control conditions ($p \leq 0.05$) and here data were analyzed

741   employing an unpaired, two-tailed Student's t-test. In A ammonia excretion rates of Δ*rhr-2* are

742   shown for worms exposed to control conditions (open bar) and during a 2 hour exposure to pH

743   5.5 and 8.0, respectively (gray bars). Here for statistical analysis a Kruskal-Wallis-Test was

744   applied with post-hoc Mann-Whitney pairwise comparisons (n= 4-6). Bars labeled with different

745   letters are significantly different. All data represent means ± SEM.

746

747   Figure 4: Representative scans showing voltage differences recorded by SIET over the

748   hypodermis for H^+ fluxes in (A) N2 worm and (B) Δ*rhr-2* at locations 100 μm or more posterior

749   to the excretory pore of adult *C. elegans*. The length of each arrow corresponds to the mean flux

750   of 3 replicate measurements at each site. Sites were separated by 25 µm. Flux scales (pmol cm^{-2}

751   s^{-1}) scales are provided in A and B.   C) H^+ fluxes (mean + SEM) for N2 worms (N = 5)

752   and Δ*rhr-2* worms (N = 5). Fluxes for each worm were calculated from the mean value for

753   measurements at 5 sites separated by 25 µm and the value at each site was the mean of 3

754   replicate measurements. The asterisk indicates a significant difference between the means (P <

755   0.005; unpaired Students t-test).

756

757 Figure 5: Specific enzyme activities of cytochrome c oxidase (A; n=5-6) and citrate synthase (B;

758 n=5-6) in fed wild type worms (N2) (open bars) and Δ*rhr-2* (closed bars). Significant differences

759 from the control value are indicated by asterisks (p ≤ 0.05). Data represent means ± SEM and

760 were analyzed employing an unpaired, two-tailed Student's t-test.

761

762 Figure 6: Changes of mRNA expression levels of *rhr-1* (n=4), *nka* (α-subunit) (n=4) and *vat*

763 (subunit A) (n=3-4), *nhx-3* (n=3-4), and *nhx-4* (n=4-5) in fed *C. elegans* wild-type worms (N2)

764 and Δ*rhr-2*. Absolute mRNA expression levels of N2 worms were set to 1 and are indicated by

765 the dotted line. Asterisks (*) indicate significant differences in mRNA expression of the

766 respective gene in N2 and Δ*rhr-2* (p ≤ 0.05). Data represent means ± SEM and were analyzed

767 employing an unpaired, two-tailed Student's t-test prior to calculation for fold change values.

768

769 Figure 7: Changes of mRNA expression levels of *rhr-1* (n=4), *nka* (α-subunit) (n=4), *vat* (subunit

770 A) (n=4), *nhx-3* (n=4), and *nhx-4* (n=4) in Δ*rhr-2* under fed (closed bars) and staved (24 hours,

771 open bars) conditions. Absolute mRNA expression levels of fed animals were set to 1 with

772 values measured under starved conditions are given as "fold changes" of the respective control

773 (closed bars). Asterisks (*) indicate significant differences between treatments (p ≤ 0.05). Data

774 represent means ± SEM and were analyzed employing an unpaired, two-tailed Student's t-test

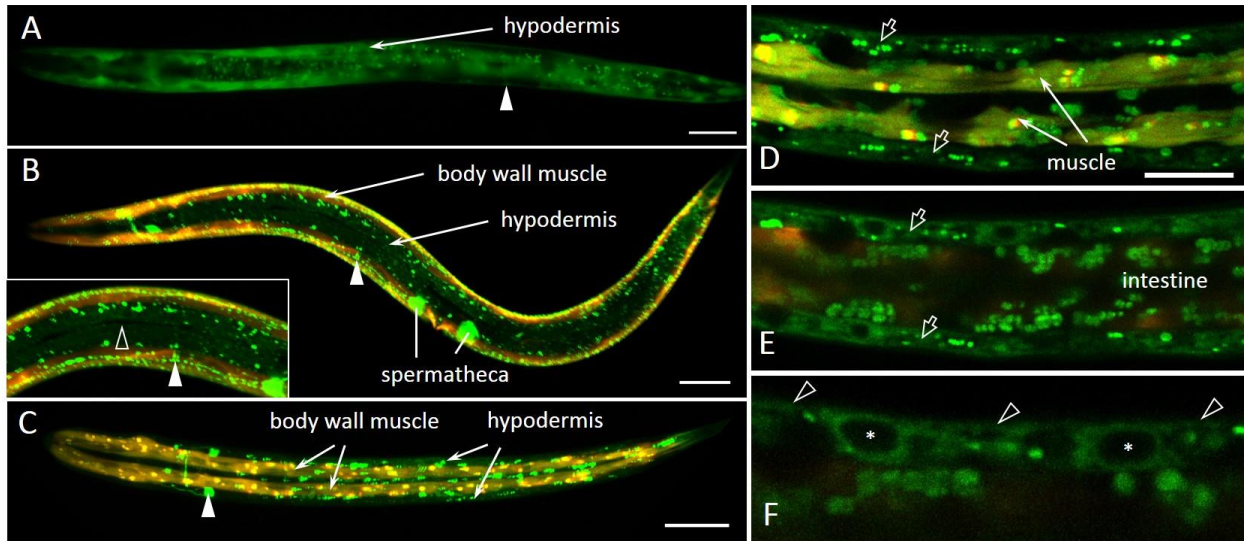775 prior to calculation for fold change values.

776

777   Figure 8: Hypothetical working model of the ammonia excretion mechanisms across the

778   hypodermis in *C. elegans*. For a detailed description refer to the text.

779

780   Supplemental figure S1: A) ClustalW amino acid alignment (Thompson et al., 1994) of *C.*

781   *elegans* RHR-1 (GenBank accession # NP_504436.1) and RHR-2 (GenBank accession #

782   NP_505961.1). Conserved ammonia-conducting residues are highlighted with a grey

783   background. Δ indicates the ammonia-conducting residues in the external vestibule; Ω indicates

784   the ammonia-conducting residues in the pore entrance; + indicates the ammonia-conducting

785   residues in the pore center; $ indicates the ammonia conducting residues in the internal vestibule

786   (Khademi et al., 2004; Zidi-Yahiaoui et al., 2009). Missing AA sequence in the Δ*rhr-2* mutant is

787   marked as bold and underlined. B) Test PCR on genomic DNA (gDNA) to confirm missing

788   nucleotide sequence in Δ*rhr-2*. The employed primer were designed to span the 750 bp deletion.

789   Lanes: M, marker; -gDNA, no DNA added to reaction; N2, PCR employing the primer pair

790   CeDel-F (5' -CACAATGGGTGTGCTATTAGG -3') and CeDel-R (5' –

791   CGAAACGTTCTCTCGATCTCC -3') and gDNA from wild-type *C. elegans*; Δ*rhr-2*, PCR

792   employing CeDel-F/-R and gDNA from the RHR-2 knock-out mutant, Δ*rhr-2*. The annealing

793   temperature were set to 60°C. C) Test PCR on cDNA to confirm missing nucleotide sequence in

794   Δ*rhr-2*. Lanes: M, marker; -RT, negative control, no DNA added to reaction; N2, PCR

795   employing the primer pair CeRhr-2 F (table 1) and CeRhr-2 R (table 1) and cDNA from N2;

796   Δ*rhr-2*, PCR employing CeRhr-2 F/R and cDNA from Δ*rhr-2*. Boxed in amino acids sequences

797   indicate location of primers employed in this reaction.

798

799

800

801   Figure 1

802

Figure 1

A hypodermis

B body wall muscle
  hypodermis
  spermatheca

C body wall muscle   hypodermis

D muscle

E intestine

F

803

804

805

806

807

808

809

810

811

812

813

814

815

816   Figure 2

817
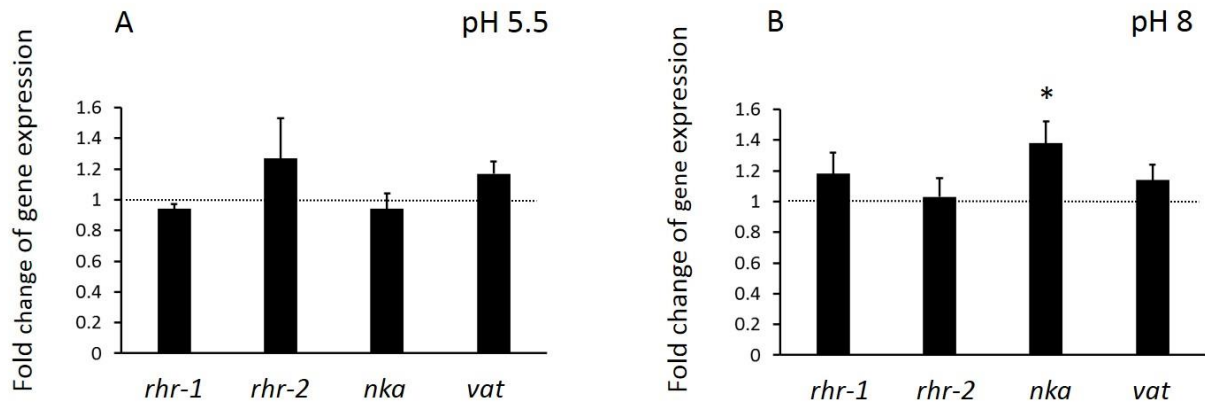
818

819

820

821   Figure 3

822

835   Figure 4

836

A   **Wild type (N2)**

B   **Δ*rhr-2***

C
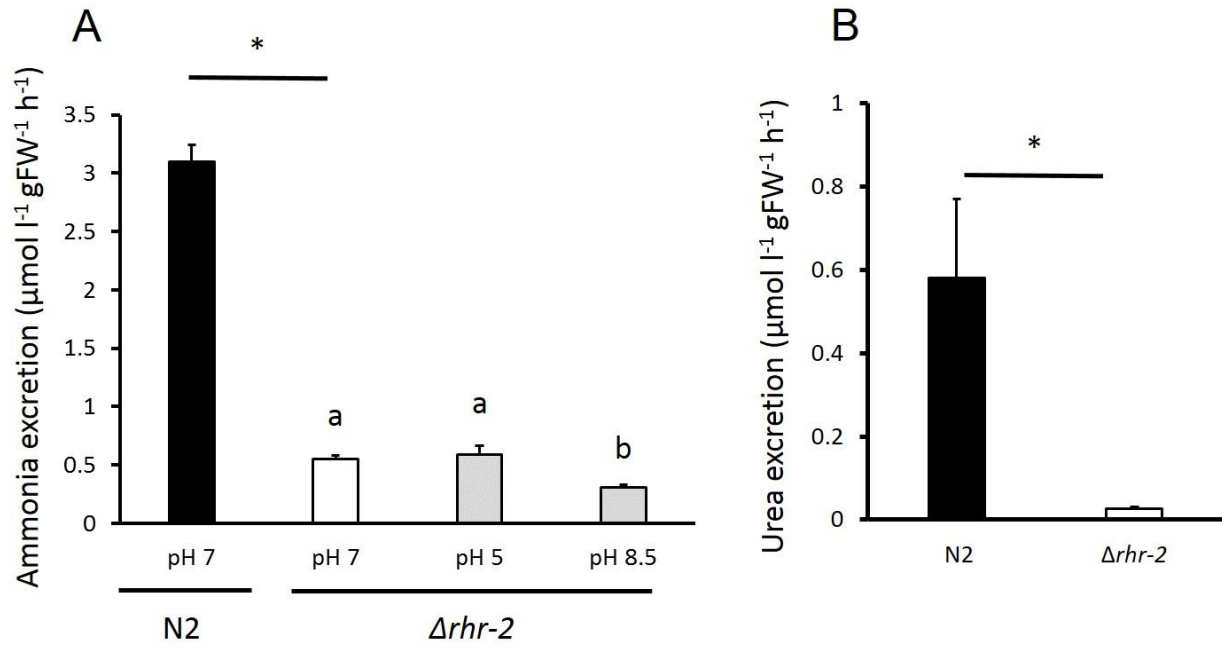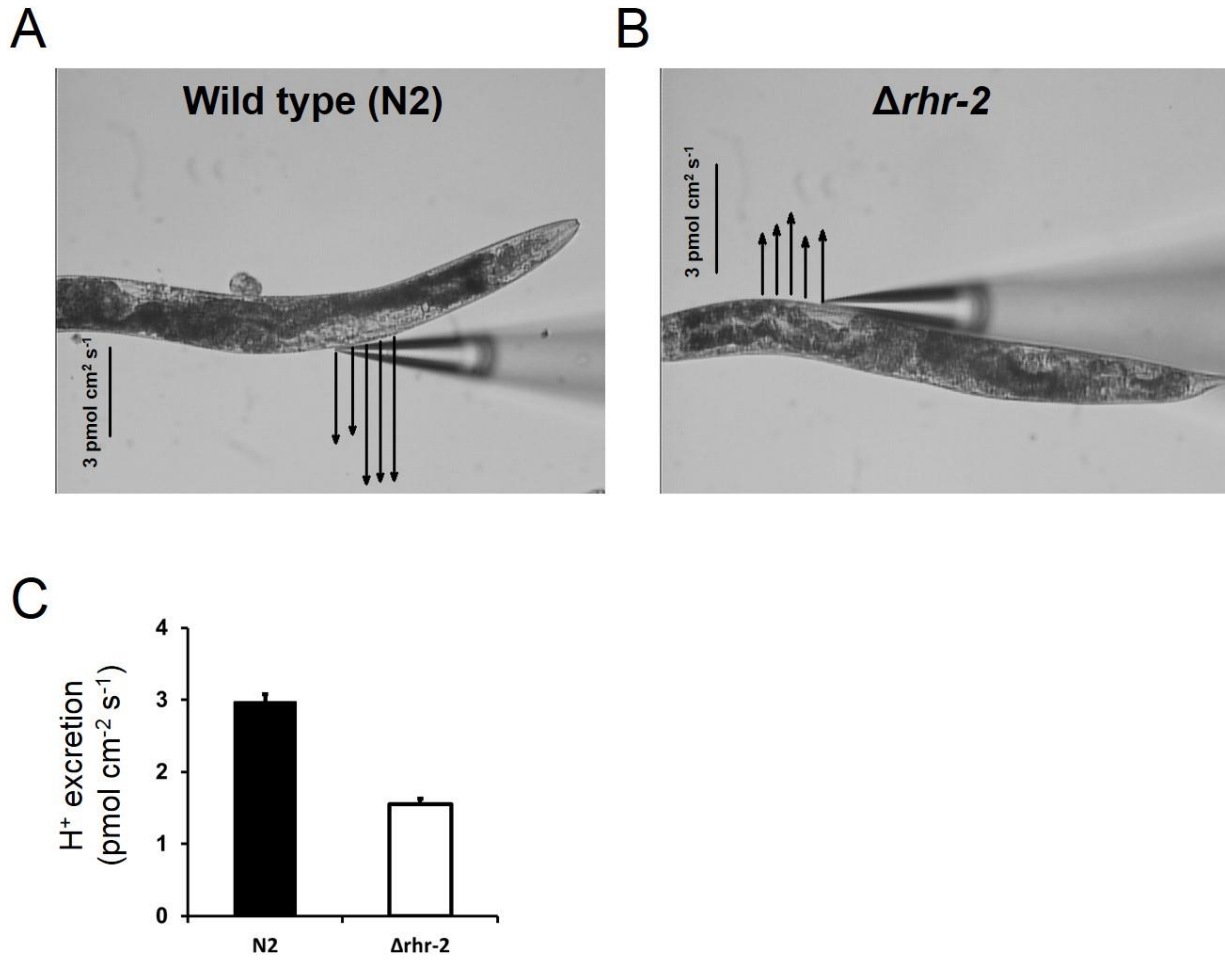
837

838

839

840

841

842

843

844

845

846   Figure 5

847

A

Cytochrome c oxidase

B

Citrate synthase
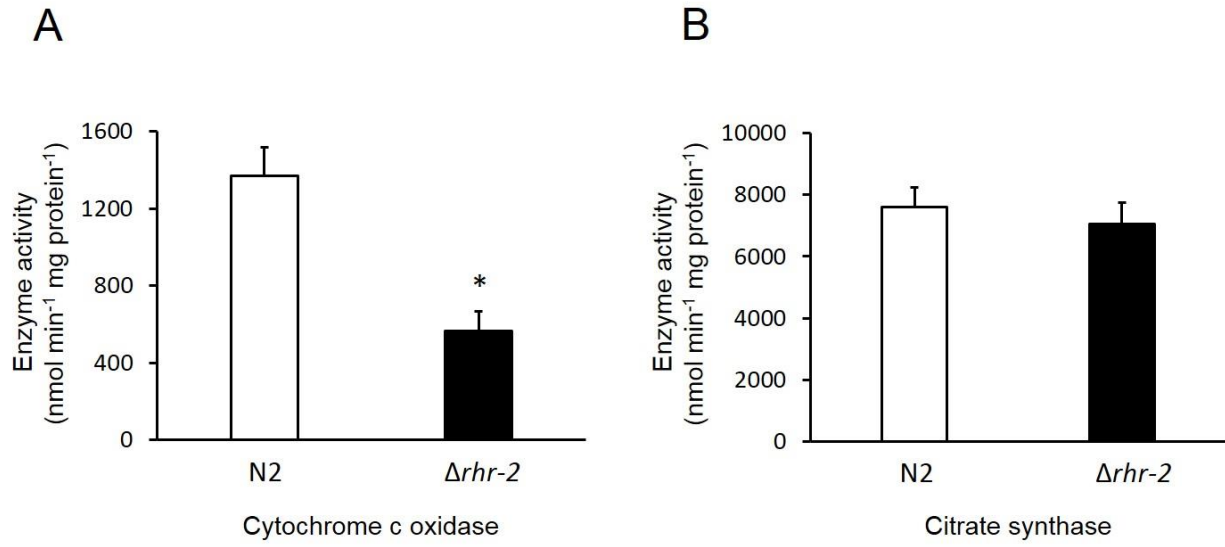
848

849

850

851

852

853

854

855

856   Figure 6

857

858
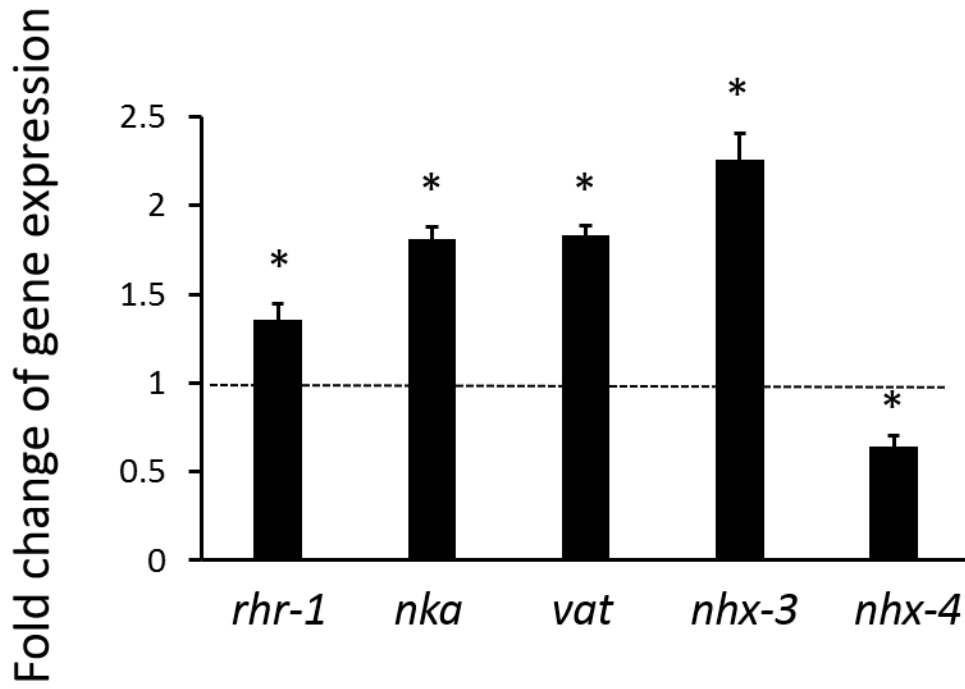
859

860

861   Figure 7

862
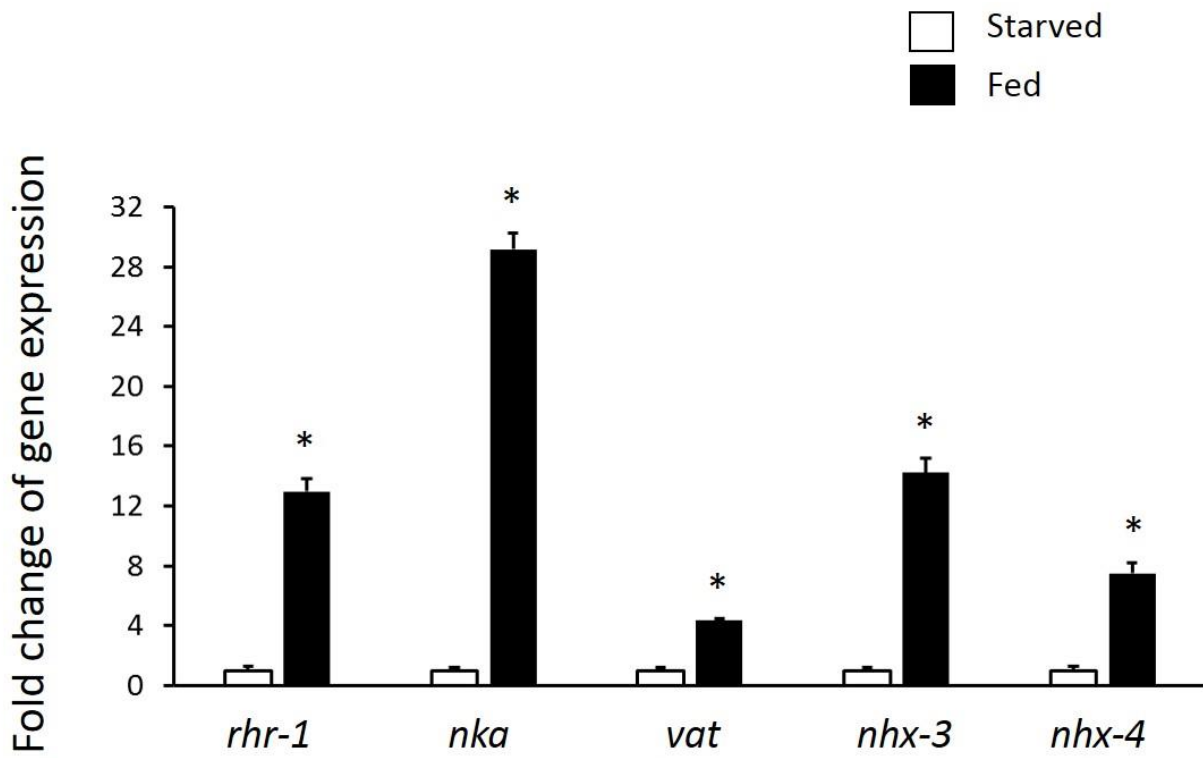
863

864

865

866

867

868

869

870

871

872   Figure 8

873
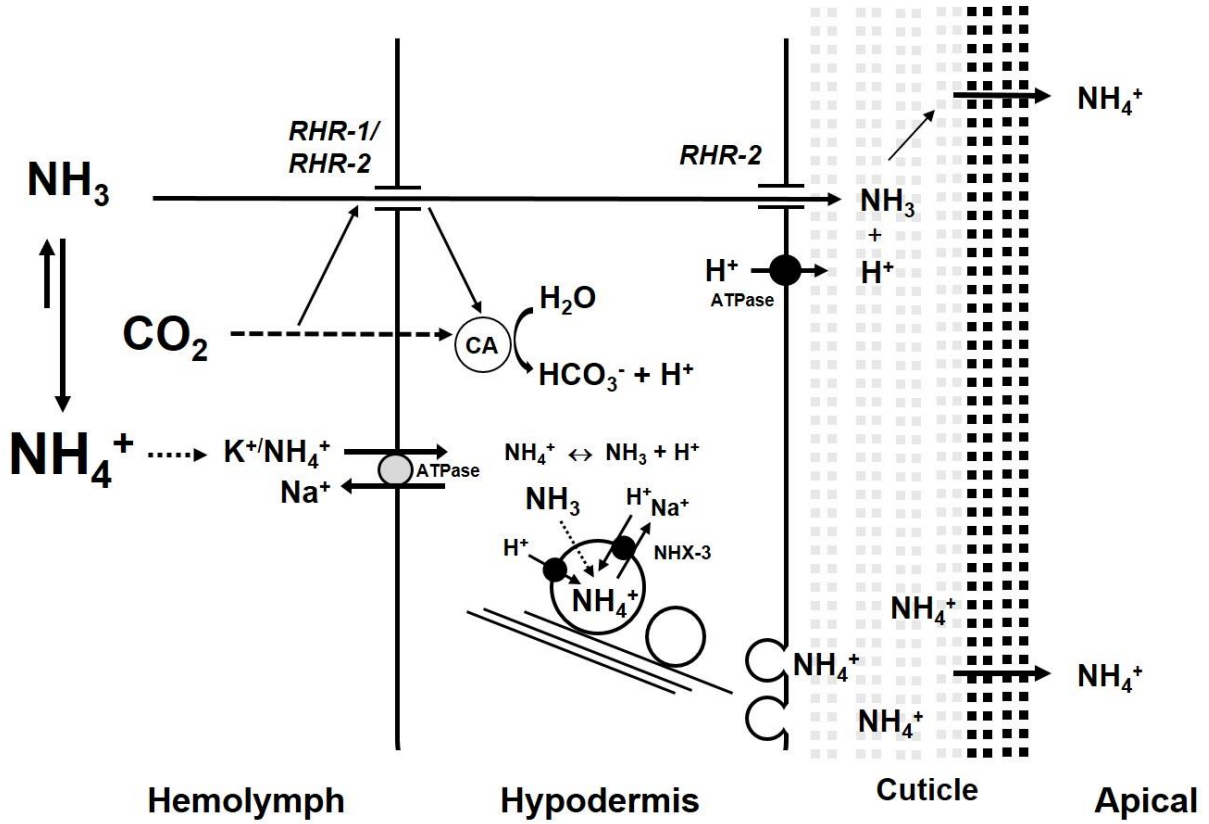
A

```
C.elegans RHR-1    MRSPLHQNQLTLILGLFQVVFLVIFALYGSYDASALPSETKNVEEAARMTNLYPLFQDTH
C.elegans RHR-2    MWSVLHRRQFAIIAGLMQTVFIVLFAKYVKYIDP--LDDSRRVYSGT----DYPLFQDVH


C.elegans RHR-1    VMIFIGFGFLMTFLKRYGFSAVSINMLLAVFTIQWGIIVRGMASAHHGFK--FTISLEQL
C.elegans RHR-2    LMIFVGFGFLMAFLKRYGFSAVSVNLLLSAFVIQFAMLLRGFMTVAFQETGLFSIGIPEM

C.elegans RHR-1    LTADFAAAVILISMGAMLGKLSPSQYVIMAFFETPVALIVEHICVHNLQINDVGGSIIVH
C.elegans RHR-2    ISAESSCAAVLITMGVLLGRLTPVQFLLLAFFETGINVLVEHYVFNYLHVNDSGRSLSVH
                   Ω                                                     Δ      +

C.elegans RHR-1    AFGAYFGLACAKGFGKKEQRGHTNEGSTYHTDIFAMIGAIFLWIYWPSFNAAVAATDDAR
C.elegans RHR-2    TFGAYFGLAAACVGHKKNVMEMDEHGGIHHSDLFSMIGTLLLWVFFPSFNAAIQEPEDAR
                                                           Ω      Δ

C.elegans RHR-1    QRAVANTFLSLCACTMTTFLVSQAVDKHKRFDMVHIANSTLAGGVAIGTTANVVLEPYHA
C.elegans RHR-2    HRAIMNTYLAMASGTVTTFMISSCVDTLGRFNMIHIQSSTLAGGVAIGSSANAVLHPYHA
                                                        $

C.elegans RHR-1    MIIGVIAGAVSVIGYKYITPFLSEKLGIHDTCGVNNLHGMPGLIAGFASIAFLFIYDETR
C.elegans RHR-2    VIVGVIAALLSVIGHAWISPRLERTFHLFDTCGVHNLHGMPGILAGLLSIGFAYFYEPES
                                                   $        +

C.elegans RHR-1    YPAQYDKIYPGMARGEDRTRMFDEKTQALNQLMAIGLVFLASTVSGYLTGLLLKLKIWDQ
C.elegans RHR-2    YGKTLYHIYPYWIGG-ELHGDRENVSQAQYQALGLLTILVTAVIGGLLTGCILKIKVWNQ

C.elegans RHR-1    VRDDEYYADGDYFETPGDYDFTSRIVTSVKQIEVAEYNPLSQKEV
C.elegans RHR-2    VDDPDFPHGEMNYYAQSDVNFLSKYKHAQEQERLREREQMQEIY-
```
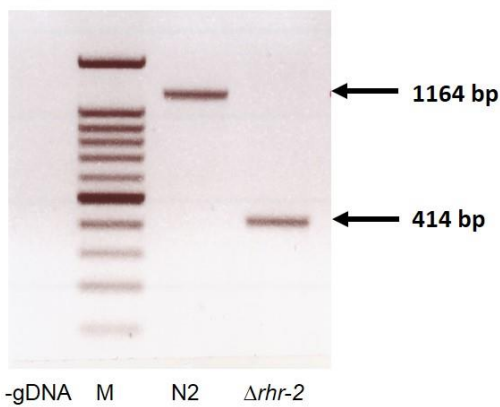
884

885

B

← 1164 bp

← 414 bp

-gDNA   M   N2   Δrhr-2

C

← 205 bp

Δrhr-2   M   N2   -RT

886

887

888